Biomaterials Science

Green and Cytocompatible Carboxyl Modified Gold-Lysozyme Nanoantibacterial for Combating Multidrug-Resistant Superbugs

Journal:	*Biomaterials Science*
Manuscript ID	BM-ART-06-2019-000935.R1
Article Type:	Paper
Date Submitted by the Author:	31-Aug-2019

Complete List of Authors:	Ahmady, Islam; University of Sharjah, Applied Biology Hameed, Mehavesh; University of Sharjah, Center for Advanced Materials Research, Research Institute for Science and Engineering, Almehdi, Ahmed; University of Sharjah, Center for Advanced Materials Research, Research Institute for Science and Engineering, Arooj, Mahreen; University of Sharjah, Center for Advanced Materials Research, Research Institute for Science and Engineering, Workie, Bizuneh; Delaware State University, Chemistry Sahle-Demessie, Endalkachew; Sustainable Technology Division, National Risk Management Research Laboratory Han, Changseok; Inha University College of Engineering, Department of Environmental Engineering College of Engineering Mohamed, Ahmed ; University of Sharjah, Center for Advanced Materials Research, Research Institute for Science and Engineering,

ARTICLE

Green and cytocompatible carboxyl modified gold-lysozyme nanoantibacterial for combating multidrug-resistant superbugs

Received 00th January 20xx,
Accepted 00th January 20xx

DOI: 10.1039/x0xx00000x

Islam M. Ahmady,[a] Mehavesh K. Hameed,[b] Ahmed M. Almehdi,[b] Mahreen Arooj,[b] Bizuneh Workie,[c] Endalkachew Sahle-Demessie,[d] Changseok Han,[e] Ahmed A. Mohamed[b,*]

The dissemination of the multi-drug resistant (MDR) superbugs in hospital environments, communities and food animals, and the very dynamic bacterial mutation frequency require the development of prolonged therapeutic strategies to gain mastery over antibiotic resistance. The AuNPs-lysozyme nanoantibacterial was fabricated by the conjugation of AuNPs-C_6H_4-4-COOH with lysozyme via the green reduction of aryldiazonium gold(III) salt [HOOC-4-$C_6H_4N{\equiv}N$]$AuCl_4$. Results from the molecular docking calculations aimed at revealing the binding mode of benzoic acid with the lysozyme structure clearly showed the lowest energy conformation with benzoic acid bounded in the deep buried hydrophobic cavity of the protein active site through strong hydrogen bonding and hydrophobic interactions, thus validating the experimental outcomes of the current study which also exhibited the binding of -COOH functional groups in the interior of the protein structure. The superiority of the lysozyme bioconjugate against superbugs was demonstrated in the enhanced and broadened lysozyme antibacterial activities of 98-99% against extended spectrum beta lactamase (ESBL) producing *Escherichia coli*, imipenem-resistant *Pseudomonas aeruginosa* clinical isolates and a selection of Gram-negative and Gram-positive standard ATCC strains. Selective toxicity against bacteria was confirmed by the high viability of HeLa and fibroblast cell lines and the outstanding hemocompatibility at the minimum bacterial inhibitory concentrations (MICs). Turbidimetric enzyme kinetic assay showed gold nanoparticles enhancement of the lysozyme hydrolytic activity on *Micrococcus lysodeikticus* bacterial substrate. Using gel electrophoresis, the induced cell wall breakdown was confirmed by detecting the leaked-out bacterial genomic DNA. The integrity and morphology change occurred to the *E. coli* bacteria were investigated using scanning electron microscope after one hour in contact with the lysozyme gold bioconjugate. The antibacterial functionalities showed little or no damage against healthy human cells and can be applied to wound dressings and medical devices.

1. Introduction

The great discovery of the super weapon-antibiotics resulted in a revolutionized medicine and significant decrease in human morbidity and mortality.[1-4] However, their exaggerated prescription as broad-spectrum antibiotics expedited their bacterial resistance. Microorganisms which develop a formidable antibiotic resistance are often coined as "superbugs".[5,6] Superbugs often carry several resistant enzymes and eventually result in apocalypse of antibiotics. One of the most common enzymes is the extended spectrum beta (β) lactamase (ESBL), which is mainly produced by Gram-negative bacteria, and can make hospitalized patients resistant to all β-lactam antibiotics including penicillin and the third and fourth generations of cephalosporin.[7] Imipenem is a broad-spectrum β-lactam antibiotic synthesized from the naturally produced antibiotic thienamycin and is the first commercially available carbapenem. Imipenem is effective against a wide range of superbugs, particularly Gram-negative bacteria in hospitals. The continuous prescription of imipenem as a broad-spectrum antibiotic to treat mixed bacterial infections resulted in vulnerability to bacterial resistance.[8] World Health Organization (WHO) listed ESBLs-producing and imipenem-resistant superbugs at the foremost priority for the development of new antibiotics to combat multidrug-resistant (MDR) bacteria.[1-6]

Enzyme proteins are used in food processing, biofuel manufacturing and as both antifouling and antimicrobial agents for surface functionalization of biomedical implants.[1,3,9-12] They are emerging green antimicrobials instead of the

[a] Department of Applied Biology, University of Sharjah, Sharjah 27272, United Arab Emirates
[b] Centre for Advanced Materials Research, Research Institute for Science and Engineering, University of Sharjah, Sharjah 27272, United Arab Emirates
[c] Department of Chemistry, Delaware State University, 1200 North DuPont Highway, Dover, Delaware 19901, United States
[d] The U.S. Environmental Protection Agency, ORD, NRMRL, LMMD, MMB, 26 W. Martin Luther King Jr. Drive, Cincinnati, Ohio 45268, United States
[e] Department of Environmental Engineering, INHA University, Michuhol-gu, 100 Inha-ro, Incheon 22212, Republic of Korea
[e.] † Footnotes relating to the title and/or authors should appear here.
[f.] Electronic Supplementary Information (ESI) available: [IR and TEM data]. See DOI: 10.1039/x0xx00000x

harmful antiseptic and disinfectant chemical agents such as chlorine, dyes, formaldehyde and detergents. Through a plethora of literature examples, it is well established that most enzymes are anchored to nanostructured surfaces and able to maintain their antibacterial activity for a prolonged time.[13-16] The biomedical activity of nanoparticles-enzyme bioconjugate is generally higher than the native enzyme and resulted in minimum inhibitory concentration (MIC) decrease and ultimately a significant drop in drug dosage in addition to the toxicity decline against human cells.[13-16]

Lysozyme protein is known to maintain relentless antibacterial activity by attacking the protective cell wall of bacteria. It catalyses the hydrolysis of the 1,4 linkages between N-acetylmuramic acid and N-acetyl-D-glucosamine residues in the peptidoglycan layer of the cell wall.[17] Peptidoglycan is the stress-bearing structure that dictates cell shape and protects the cell wall against intracellular osmotic pressure and environmental stress.[18,19] This hydrolysis leads to cell wall loss and shape change to protoplasts in Gram-positive and spheroplasts in Gram-negative, which are osmotic sensitive forms of bacteria, thus subjected to cell lysis.[20,21]

Lysozyme possesses green antibacterial, anti-inflammatory and antiviral properties, which boost its applications in the pharmaceutical industry. It is a monomeric globular protein with an isoelectric point of 10.6 and, therefore, carries a positive charge at neutral pH. Electrostatic interaction between the positive lysozyme and the negative bacterial cell wall probably plays a significant role in the catalysed hydrolysis.[22]

In this study, we developed a green platform based on the robust Au-C nanoparticles modified with -COOH functional groups and conjugated with lysozyme aimed at controlling free floating bacterial growth. The fabrication of the gold-lysozyme bioconjugate was easily achieved under green reduction conditions of $[HOOC\text{-}4\text{-}C_6H_4N{\equiv}N]AuCl_4$ using the reducing lysozyme protein. The robust nanoparticles with direct gold-to-carbon σ-bond are hemocompatible and stable under physiological conditions.[23-26] We investigated the increase in lysozyme hydrolytic activity after conjugation with gold nanoparticles on *Micrococcus lysodeikticus* bacterial substrate using turbidimetric assay. The bioconjugate antibacterial activity was examined and the minimum inhibitory concentrations (MICs) and minimum bactericidal concentrations (MBCs) were estimated against a selection of microorganisms including extended spectrum beta lactamase (ESBL) producing *Escherichia coli*, imipenem-resistant *Pseudomonas aeruginosa* clinical isolates and Gram-negative standard strains *Escherichia coli* ATCC 25922, *Salmonella typhimurium* ATCC 29629 and *Klebsiella pneumonia* ATCC 13833 and Gram-positive *Staphylococcus aureus* ATCC 29213. The morphological changes of ESBL-producing *E. coli* and adsorption of AuNPs-lysozyme nanoparticles to the bacterial cell wall were probed with scanning electron microscope. Moreover, cell wall breakdown was confirmed by detecting the leaked-out bacterial genomic DNA by agarose gel electrophoresis. Toxicity to human tissues was assessed *in vitro* against human fibroblast and HeLa cancer cells using tetrazolium dye MTT colorimetric assay, and cellular morphologies were assessed after 24 h of incubation. The hemocompatibility of the bioconjugate was evaluated after 1 and 24 h of incubation.

It is imperative to understand the important phenomena that how after binding with the negatively charged nanoparticles, lysozyme is still able to maintain its electrostatic interactions with the negatively charged bacterial wall instead of being repelled. Molecular docking is an effective and competent tool which can be helpful to get insights into the binding mechanism of molecules by predicting the preferred relative orientation of one molecule in the active site of another molecule to form a stable complex with lowest free energy.[27-29] Therefore, molecular docking studies were performed to get molecular level details of the lysozyme binding with -COOH functional groups. Lysozyme structure complexed with benzoic acid may give insights into how positively charged globular protein binds with benzoic acid and what kind of molecular surface of lysozyme is left to be exposed to the negatively charged bacterial wall after binding with benzoic acid.

2. Experimental

2.1. Materials

Lysozyme from chicken egg white powder, Dulbecco's Modified Eagle's Medium-high glucose (DMEM), tetrazolium dye [3-(4,5-dimethylthiazol-2-yl)-2,5-diphenyltetrazolium bromide] (MTT), fetal bovine serum (FBS), trypan blue, potassium phosphate monobasic and dibasic, agarose and TAE buffer (pH 8.3) from Sigma-Aldrich. Phosphate buffer saline of pH 7.4 (1X PBS) and Penicillin-Streptomycin (Pen-Strep) from Gibco by life technology. Nutrient and Muller-Hinton agars and broth from HIMEDIA, India. Ethidium bromide, 5X DNA loading buffer and 1Kb DNA ladder from Bioline.

2.2. Bacterial strains, cell lines and red blood cells

Gram-negative and Gram-positive bacterial strains from ATCC. Gram-negative bacterial strains are *Escherichia coli* ATCC 25922, *Salmonella typhimurium* ATCC 29629 and *Klebsiella pneumonia* ATCC 13833 and Gram-positive bacterial strain is *Staphylococcus aureus* ATCC 29213 and *Micrococcus lysodeikticus* ATCC 4698 from Sigma-Aldrich. Gram-negative resistant bacterial strains ESBL-producing *Escherichia coli* and imipenem-resistant *Pseudomonas aeruginosa* clinical isolates from the University of Sharjah hospital laboratory. Primary Dermal Fibroblast Normal, Human, Neonatal (HDFn) (ATCC® PCS-201-010™) and HeLa (ATCC® CCL-2™) cell lines from ATCC. Red blood cells (RBCs) were taken from the first author (IA). All experiments were performed in accordance with the Declaration of Helsinki Guidelines, and Experiments were approved by the ethics committee at the University of Sharjah (REC-19-09-22-01). Informed consents were obtained from human participants of this study.

2.3. Characterization

UV-Vis absorption spectra were recorded using Scanning Spectrophotometer (Spectro UV-2510TS, Labomed Inc) in the 200-800 nm range with 2 nm resolution. Attenuated total reflectance Fourier transform infrared (ATR-FTIR) spectra were recorded using a Burker (Platinum ATR) Tensor II FT-IR spectrophotometer. ζ-potential analysis of the nanoparticles in water was carried out using Nanotrac Wave II, model MN42x, USA. A JEOL JEM-2100 transmission electron microscope was used to investigate the morphology of the nanoparticles. Dispersed nanoparticles in acetonitrile were immobilized on 400 mesh copper grids coated by FORMVAR carbon film (FCF 400-Cu, Electron Microscopy Sciences, Hatfield, Pennsylvania, USA). MTT colorimetric assay and hemolysis estimation measured using Thermo Scientific Multiskan GO micro plate spectrophotometer. Bacterial inoculum turbidity was adjusted by DensiCHEK plus from BIOMREIUX. Turbidimetric enzyme kinetic assay with bacterial substrate was measured with BioTek spectrophotometer. Cells morphological studies were carried out using Olympus microscope IX53 model attached to a high-definition camera model DP74 of 1920 x 1200-pixel. Scanning electron microscopy (SEM) images were collected using a VEGA3 system from TESCAN and operating at 30 kV.

2.4. Green synthesis of AuNPs-lysozyme bioconjugate

Gold-aryl nanoparticles modified with carboxyl functional groups were conjugated with lysozyme by mixing an aqueous solution of 20 mL of 1×10^{-4} M lysozyme with 20 mL of 1×10^{-2} M of the aryldiazonium gold(III) salt [HOOC-4-$C_6H_4N{\equiv}N$]$AuCl_4$. The pH was adjusted to 12 using 0.1 M NaOH solution. The mixture was stirred overnight at room temperature after which it turned cherry red. Purification was carried out using similar procedure we used in our previous work.[24]

2.5. Molecular docking and molecular electrostatic potential (MEP) calculations

In this study, AutoDock 4.2 was used to prepare complex structure of lysozyme and benzoic acid.[30] The initial 3D coordinates of lysozyme protein structure were taken from the Protein Data Bank as entry 2VB1.[31] In order to prepare the protein structure for docking, heteroatoms and water molecules were removed and Kollman charges were added. 3D structure of benzoic acid was retrieved from PubChem.[32] To prepare the ligand for docking, Avogadro program (http://avogadro.cc/) was used. After preparation of both protein and ligand structures, blind docking technique was used to predict the binding mode of benzoic acid with lysozyme.[33] In order to perform blind docking, whole protein surface was scanned to find most probable binding mode of ligand at protein by setting the grid dimensions to be 74 × 104 × 106 Å. Energy evolutions of 2,500,000 were performed to search the free energy minimum of the protein-ligand complex using Lamarckian genetic algorithm of AutoDock. Generated conformations of lysozyme and benzoic acid were analysed using Discovery Studio Visualizer program.

2.6. Molecular electrostatic potential (MEP) calculations

Final conformation selected form detailed analysis of molecular docking results with lowest binding energy of -4.694. kJ/mol was subjected for MEP calculations. The macromolecular electrostatics calculation program, Adaptive Poisson-Boltzmann Solver (APBS) implemented in PyMOL, was used to perform these calculations.[34] The electrostatic potential was calculated by solving the nonlinear Poisson-Boltzmann equation using finite difference method of APBS. PB2PQR Server was used to map the electrostatic potential onto the molecular surface of the protein with a potential range from -5 eV to +5 eV. PyMOL was used to visualize the results as a color-coded electrostatic surface.

2.7. Turbidimetric enzyme activity assay with bacterial substrate

First, we investigated the increase in lysozyme hydrolytic activity after conjugation with gold nanoparticles by turbidimetric assay, in which the decrease in optical density (OD) of an aqueous suspension of Gram-positive *Micrococcus lysodeikticus* (ATCC 4698) in potassium phosphate buffer was monitored for 5 min. *Micrococcus lysodeikticus* is a natural substrate for lysozyme.[35] The reduction in the optical density indicates the hydrolysis of peptidoglycan layer due to the breakdown of 1,4 linkages between N-acetylmuramic acid and N-acetyl-D-glucosamine residues. Assay method was done following the manufacture instructions, one unit of lysozyme will produce a decrease of 0.001 in OD per minute at 450 nm under conditions of pH 6.24 at 25 °C in a 2.6 mL reaction mixture and light path of 1 cm. We used the same conditions and reaction mixture of 260 µL.[36] Briefly, 50 mM potassium phosphate buffer (pH 6.24) was prepared by adding 20.125 mL of 1.0 M potassium phosphate monobasic solution to 7.375 mL of 1.0 M potassium phosphate dibasic solution, the final volume was adjusted to 550 mL with ultrapure distilled water and pH was adjusted using 1 M HCl or 1 M NaOH. A suspension of *Micrococcus lysodeikticus* was prepared in the buffer, initial OD was adjusted in the range 0.6-0.7 at 450 nm, then 10 µL of AuNPs-lysozyme was added to 250 µL of bacterial suspension in a 96-well microplate at 25 °C and the decrease in OD at 450 nm was monitored for 5 min. Kinetic curve of *Micrococcus lysodeikticus* lysis was constructed as OD vs. time in minutes. Reduction in the absorbance (ΔA_{450}) vs. time curve was generated. Kinetic experiments were reproduced in triplicate. Percentage of enzyme activity in the first minute of the reaction was measured using Equation 1

$$\text{Units mL}^{-1}\text{ enzyme} = \frac{\Delta A450\ \text{test/min} - \Delta A450\ \text{blank/min}}{0.001 \times 0.01} \times df \qquad (1)$$

where df = dilution factor, 0.001 = change in absorbance (ΔA_{450}) as per the unit definition and 0.01 = volume in millilitre of enzyme solution.

2.8. Determination of encapsulation efficiency (EE) of lysozyme bioconjugate

To estimate the loading efficiency of lysozyme in the bioconjugate, we centrifuged the solutions at 14000 rpm for 30 min at 4 °C. Supernatants were decanted after centrifugation. Protein content in the supernatants was quantified by Bradford protein assay using UV spectrophotometer at 595 nm.[24] Samples were prepared and measured in triplicate. The encapsulation efficiency was calculated using Equation 2.

$$\text{EE \%} = \frac{\text{Total amount of lysozyme added} - \text{Free lysozyme}}{\text{Total amount of lysozyme added}} \times 100 \qquad (2)$$

2.9. Minimum inhibitory concentration (MIC)

Clinical and Laboratory Standards Institute (CLSI) guidelines were followed to detect the minimum concentration of antibacterial agent that completely inhibits the bacterial growth (MIC).[37] Native lysozyme, AuNPs-COOH and AuNPs-lysozyme bioconjugate were diluted in Muller Hinton broth in the microtitration plate. Each sample was tested in triplicate. The sterility of the solutions was tested by spreading 100 µL on nutrient agar and incubated for 24 h.

Standard inoculum of the testing microorganisms was prepared in a saline solution from 24 h agar plate using the direct colony suspension method. Inoculum optical density was adjusted at 600 nm using DensiCHEK to give a concentration of 1×10^8 CFU mL^{-1} equivalent to 0.5 McFarland standard solutions. It was further diluted to give a final bacterial concentration of 5×10^5 CFU mL^{-1} in 100 µL of the diluted testing solutions. Control wells of broth with bacteria and sterility wells containing broth only were prepared. The plates were sealed and incubated overnight in a shaking incubator at 37 °C. MIC was visually detected. The growth amount in the testing solution wells was compared with the growth amount in the control wells to determine the growth end points. Control of ≥2 mm button or definite turbidity in the control wells is considered an acceptable growth.

2.10. Minimum bactericidal concentration (MBC)

The minimum concentration that kills 99.9% of the initial inoculum was detected following CLSI guidelines.[38] Typically, 10 µL from all wells, which showed inhibition of growth after 24 h were sub-cultured onto nutrient agar and incubated for 24 h at 37 °C.

2.11. Detection of bacterial DNA leakage

To confirm the cell wall breakdown by AuNPs-lysozyme bioconjugate, we examined the leakage of bacterial genomic DNA with agarose gel electrophoresis. We followed a previous protocol with some modifications.[26] Typically a standard bacterial suspension of 1×10^8 CFU mL^{-1} was prepared for all tested strains in phosphate buffer, then 100 µL of the suspension was incubated with 50 µL of lysozyme and AuNPs-lysozyme bioconjugate for 3 h at 37 °C in shaking incubator at 100 rpm. Then samples were centrifuged for 1 min at 11,000 rpm and 25 µL of supernatant was added to 3.5 µL loading dye from Bioline and loaded onto 1% agarose gel in 100 mL of TAE buffer containing 2 µL of 1 µg/mL ethidium bromide to view the leached DNA bands. Electrophoresis was carried out for 50 min at room temperature under a constant electric field of 100 V in electrophoresis apparatus from Bio-Rad. Pictures of DNA bands were photographed by gel documentation system from Bio-Rad. The experiment was reproduced in triplicate.

2.12. Nanoparticles adsorption to bacterial cell wall

Adsorption of the AuNPs-lysozyme to bacterial cell wall and cellular physical changes were examined using SEM. A 50 µL of standard inoculum of ESBL-producing *Escherichia coli* strain 1 was incubated with 200 µL of 50% concentration of lysozyme and 50% AuNPs-lysozyme bioconjugate in Muller Hinton broth for 1 h at 37 °C shakier at 100 RPM. Then 10 µL was placed on the specimen stage and kept without disturbance for air dry and inspected using SEM. Control sample of *E. coli* was examined with SEM to confirm the rod shape of the strain (picture not included).

2.13. MTT colorimetric assay for testing HeLa and fibroblast cell lines cytotoxicity and cellular morphological study

MTT assay was performed on HeLa and fibroblast cell lines. The cells were cultured as ATCC recommendations in DMEM supplemented with 10% FBS and 2X Pen-Strep. HeLa cells were used at seeding density of 5×10^4 cells per well and fibroblast cells were used at 3.5×10^4 cells per well in 96 well plate,[39] and allowed to adhere for 24 h at 37 °C in a humidified atmosphere incubator with 5% CO_2 (viability of the cells used in all experiments exceeded 95% with Trypan Blue method). The medium was replaced with 100 µL of the medium contained decreased concentrations including native lysozyme, AuNPs-lysozyme bioconjugate and of the testing solution in DMEM medium and incubated for 24 h. The wells were then washed with 100 µL of PBS for 1 min. A 100 µL of the medium with 10 µL of 0.5 mg/mL MTT tetrazolium dye was incubated for 3 h. The formation of dark purple formazan crystals was observed under optical microscope. The medium was replaced with 100 µL of DMSO to dissolve the formazan crystals and the plate was shaken for 15 min. The absorbance was then measured at 570 nm using UV instrument. Cells with DMEM medium were used as the positive control, and wells with MTT reagent and DMSO were used as the negative control. High UV-Vis absorbance indicates high viability. Experiments were conducted in triplicate and cell viability % was calculated from the mean of three replica using Equation 3

$$\text{Cell viability \%} = \frac{\text{Sample abs} - \text{Negative control abs}}{\text{Positive control abs} - \text{Negative control abs}} \times 100 \qquad (3)$$

To study cellular morphological changes, HeLa and fibroblast cells were seeded at low density in tissue culture dishes of 35 × 10 mm diameter and treated with DMEM medium of MIC of the testing solutions and incubated for 24 h, and then they were washed with PBS for 2 min and viewed under phase contrast microscope.

2.14. Hemocompatibility study

The percentage of hemolysis and red blood cells (RBCs) morphological changes were detected following the protocol we used before and after some modifications.[24] Quantitative estimation of haemoglobin leached out was tested on O-positive blood group collected in EDTA. RBCs were separated from the plasma by centrifugation at 1500 rpm for 5 min and washed 3 times with PBS. Then, 200 µL of 5% RBCs in PBS was added to 800 µL of the lysozyme bioconjugate at different MICs. Samples were incubated overnight in a water bath at 37 °C and shaken gently. A 20 µL of each sample was then transferred to a microscope slide and viewed under phase contrast microscopy at a magnification of 40X. The number of haemolysed RBCs was counted per 200 cells. Morphological changes were examined after 1 h of interaction. The quantitative measurements were estimated after 1 and 24 h. Samples were centrifuged at 2500 rpm, and 100 µL of the supernatant solution was transferred to a microtitration plate. Absorption values were measured in the range of 400-700 nm. The percentage of leached haemoglobin was measured at 575 nm using microplate spectrophotometer. Hemolysis % was calculated using Equation 4

$$\text{Hemolysis \%} = \frac{\text{Sample abs} - \text{Negative control abs}}{\text{Positive control abs} - \text{Negative control abs}} \times 100 \qquad (4)$$

2.15. Statistical significance

Viability statistical significance difference was calculated using Student-t tests. Samples statistically different from controls were marked on the figures with (∗) to represent P-values <0.05 and (∗∗) to represent P-values <0.01. Cross error bars represent standard deviation of three replicas.

3. Results and discussion

3.1. Green synthesis and characterization of AuNPs-lysozyme bioconjugate

Mediated protein fabrication of nanoparticles is more biomedically friendly than chemical-based due to slower kinetics and better control over the construction of the bioconjugates.[40,41] In addition, proteins do not impose cytotoxicity under physiological conditions because of the absence of the typical chemicals involved in the nanoparticles synthesis such as phase-transfer and external chemical reducing agents. The aryldiazonium gold(III) salt was incubated with lysozyme while stirring in water during which a cherry red colour was developed (Fig. 1a). It is worth to mention the stretching frequencies of AuNPs-COOH. ATR-FTIR of the parent nanoparticles shows the presence of the carbonyl stretching at 1685 cm^{-1} and C=C stretching at 1566 cm^{-1} (Fig. S1). Solid state ATR-FTIR spectrum of lysozyme bioconjugate is comparable to that of pure lysozyme (Fig. S2). The characteristic bands of lysozyme such as amide-I at 1653 cm^{-1}, amide-II at 1540 cm^{-1} and amide-III at 1252 cm^{-1} can be clearly seen in the spectrum (Fig. S3). This supports the surface adsorption of lysozyme on AuNPs-COOH.[42] The green reduction of the aryldiazonium gold(III) salt using lysozyme resulted in the disappearance of the diazonium peak at 2268 cm^{-1}.

The blue shift in the plasmon peak from 550 nm for the gold nanoparticles to 520 nm for the lysozyme bioconjugate is due to the basic conditions of pH 12 (Fig. 1b). The blue shift was obvious in the basic media probably due to more uniform size of the gold nanoparticles after conjugation with lysozyme which is also manifested in the sharp peak compared to the broad peak of the gold nanoparticles due to the polydispersity nature or aggregation. The findings are reminiscent of the pH effect on bovine serum albumin (BSA) bioconjugate which showed a correlation between the pH change and the UV-Vis shift.[24] The fabrication of gold nanoparticles was reported involving lysozyme as the sequester and the reducing agent for gold(III) salt to gold(0) at 40 °C under microwave irradiation at pH 12.[43] In another study, the lysozyme-dextran nanogels were used to reduce the tetrachloroaurate(III) precursor under UV irradiation at pH 4.[44] In our earlier attempts to construct pure gold nanoparticles for medical applications, we used femtosecond laser ablation technique for the synthesis of ultrapure robust gold-aryl nanoparticles.[44] Laser irradiation of aryldiazonium tetrachloroaurate(III) salt fabricated Au-C nanoparticles without the need for external reducing agent or surfactant and thus purification is not of concern.[45]

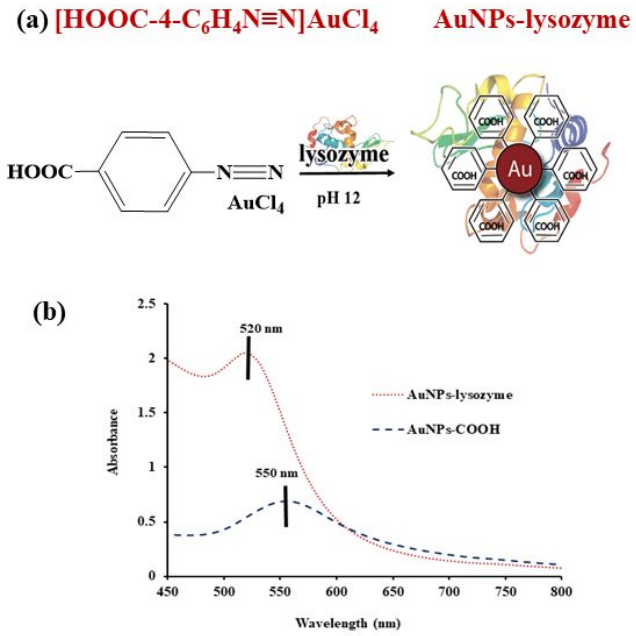

Fig. 1 (A) Fabrication steps of AuNPs-lysozyme bioconjugate. (B) UV-Vis of AuNPs-COOH and AuNPs-lysozyme bioconjugate at pH 12 showing a blue shift in the plasmon peak from 550 nm for the gold-aryl nanoparticles to 520 nm after conjugation with lysozyme.

Nanoplatform ζ-potential net charge is critical in predicting the electrostatic attraction with the negatively charged bacterial cell wall. Gold-aryl nanoparticles possess negative ζ-potential of -85.4 ± 0.8 mV under basic conditions of pH 12. Bioconjugation of the positively charged lysozyme with the negatively charged nanoparticles resulted in reversing their negative charge and acquiring a total positive zeta potential

value of +69.6 ± 0.6 mV. The high ζ-potential implies high bioconjugate stability.

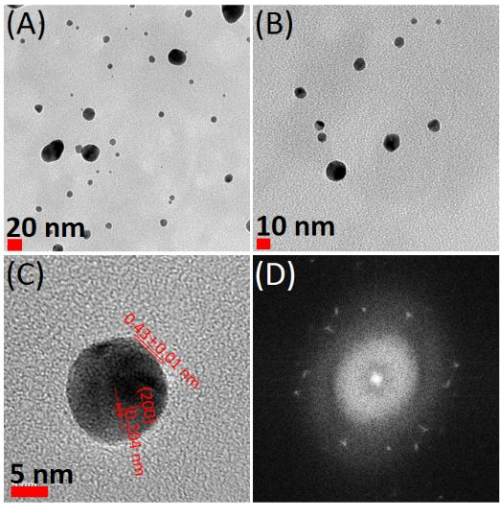

Fig. 2 HR-TEM images of AuNPs-lysozyme bioconjugate showing spherical bioconjugate without aggregation of gold nanoparticles. (A) Large nanoparticles with size of 18 nm ± 10 nm. (B) Small nanoparticles with size of 8 ± 4 nm. (C) A very thin coating of about 0.4 nm outside the gold nanoparticles. (D) Bright dots of Fast Fourier Transform (FFT) image.

The morphology of the bioconjugate was probed using HR-TEM (Fig. 2a-d). TEM images revealed successful conjugation of the gold nanoparticles with lysozyme. Spherical AuNPs-lysozyme bioconjugate is observed. Due to the formation of large particles, overall particles size was 18 ± 10 nm, but the size of small nanoparticles was 8 ± 4 nm. A very thin coating of about 0.4 nm outside the gold nanoparticles is visible in the images (Fig. 2c). As seen in Fig. 2a-b, due to the formation of lysozyme coating on the nanoparticles, no aggregation of gold nanoparticles was observed. The measured lattice spacing of 0.204 nm, corresponding to (200) plane of gold.[46] Fig. 2c indicates that gold(III) ions were effectively reduced by the green synthesis method and the observed bright dots in Fig. 2d of fast Fourier transform (FFT) images for Fig. 2c also confirmed that gold(III) ions were fully crystallized by lysozyme. The less faceted shapes indicate the lysozyme concentration to AuNPs-COOH nanoparticles is optimum to behave as a shape-directing macromolecule. Additional image showing more gold-lysozyme bioconjugate nanoparticles is included in the supporting information (Fig. S4).

3.9. Molecular docking calculations

Present molecular docking study is aimed to reveal the binding of benzoic acid to the positively charged globular lysozyme protein. The final binding mode of benzoic acid to lysozyme with lowest free energy of -4.694 kJ/mol was selected for detailed analysis. Benzoic acid is bounded well in the deep hydrophobic cavity of lysozyme and showed key interactions with the active site region of the protein.[47] A strong hydrogen bonding interaction with 1.93 Å between the hydrophobic residue Ala107 and hydrogen from benzoic acid was observed. Along with this key hydrogen bonding interaction, hydrophobic interactions between benzoic acid and the hydrophobic residues of the active site of lysozyme such as Ile58, Ala107 and Trp108 were observed (Fig. 3). The benzene ring of the benzoic acid also formed π-π T-shaped stacking interactions with the side chain of aromatic residue Trp108 which is located in the hydrophobic matrix box of protein structure. Previous studies speculated that Trp108 is one of the most dominant fluorophores in lysozyme.[48,49] Asn59 from the active site of lysozyme also formed interactions with benzoic acid. All these residues including Ile58, Asn59, Ala107 and Trp108 are located at the cleft of the receptor protein and considered important for the optimal binding of the ligand at the active site of lysozyme.[47,50,51] In order to reveal the nature of the electrostatic potential surface of the binding pocket of lysozyme exposed to the ligand, the mapping of the electrostatic potential onto the molecular surface of the protein with a potential range from -5 eV to +5 eV was performed and analysed. The color-coded electrostatic surface of lysozyme clearly exhibits the binding of benzoic acid in the deep buried cavity of protein structure (Fig. 3). This surface presentation also aids in the interpretation of the positively charged globular protein in terms of its ability to form strong electrostatic interaction with the negatively-charged bacterial cell wall. We can clearly see the positively-charged surface of protein color-coded with blue is present at the outer surface and the negatively charged hydrophobic cavities color-coded with red are buried inside the interior of the protein. The findings from this study clearly show the binding of benzoic acid into the buried cavity of the active site of lysozyme, thus validating the experimental results from this study which also show that the nanoparticles are attached at the interior side of the lysozyme protein.

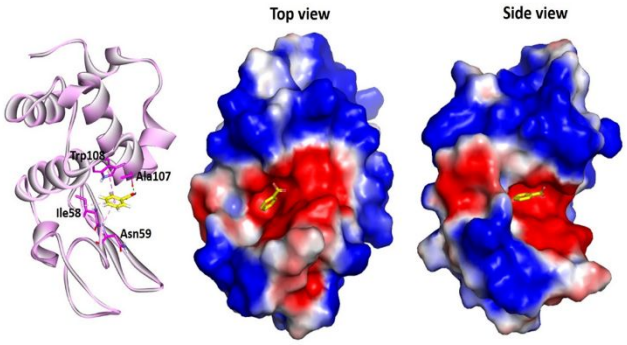

Fig. 3 Complex of benzoic acid with lysozyme. Structure of lysozyme shown in pink coloured ribbon presentation. Residues involved in interaction with benzoic acid are shown in pink coloured stick style. Only polar hydrogen atoms are shown for clarity. Hydrogen bonding and hydrophobic (including π-π) interactions are indicated using green and pink dashed lines, respectively. Electrostatic potential surface obtained by APBS. Contour level for the electrostatic potential at the solvent-exposed surface is set to -5 (red) and +5 (blue) K_bT/e_c. Benzoic acid is shown as yellow stick style.

3.2. Measurement of enzyme hydrolytic activity increase

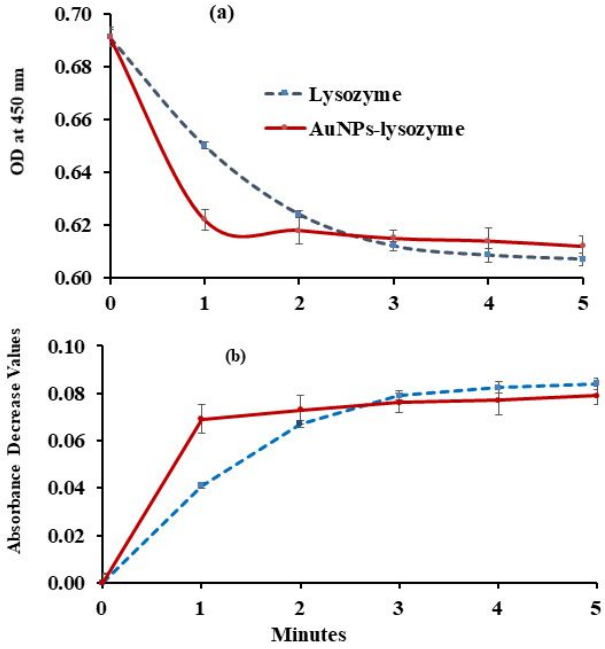

Fig. 4 Turbidimetric assay with *Micrococcus lysodeikticus*. (a) Kinetic curves show faster reduction of the substrate optical density in the first two min of the reaction with AuNPs-lysozyme compared to native lysozyme. (b) Graph of the reduction in the optical density (ΔA_{450}) for both AuNPs-lysozyme bioconjugate and native lysozyme. Concentration is 10 μL of 1.43×10^4 μg/μL.

Enhancement in lysozyme hydrolytic activity was measured by turbidimetric assay, which was performed by monitoring the decrease in the optical density of *Micrococcus lysodeikticus* suspension at 450 nm for lysozyme bioconjugate and native lysozyme.[27] Lysozyme cleaves the β (1–4) glyosidic bond between N-acetylmuramic acid and the N-acetyl-D-glucosamine in the polysaccharide that forms peptidoglycan the backbone layer of bacterial cell walls.[19,35] This cleavage is the first step in the lysis of bacterial cells. The degree of lysis is measured as reduction in turbidity of the bacterial suspension.[35,36,52,53] The decrease in substrate optical density was measured at 450 nm (Fig. 4a). The reduction in the absorbance (ΔA_{450}) vs. time was generated (Fig. 4b). We observed significant and fast bacterial degradation for lysozyme bioconjugate. Native lysozyme measured an activity of 41,000-unit mL^{-1}, while the bioconjugate measured 69,000 unit mL^{-1} in the first minute of the reaction. An increase of 68% in the hydrolytic activity was calculated. This increase in enzyme activity against bacterial substrate is mostly because of the increase in the adsorption of lysozyme to the negative cell wall. This finding is similar to the results obtained by others in which they have shown that the activity of lysozyme was enhanced after attachment to silver, latex and gold nanoparticles.[19,36,52-54]

3.3. MIC and MBC estimation

Table 1. MIC and MBC values of AuNPs-COOH, AuNPs-lysozyme bioconjugate and native lysozyme in μg mL^{-1}

Strain	AuNPs	AuNPs-lysozyme MIC	AuNPs-lysozyme MBC	Lysozyme MIC	Lysozyme MBC
E. coli ESBL 1	-*	0.49	62.0	1.07×10^4	-
E. coli ESBL 2	-	0.49	62.0	0.78×10^4	1.07×10^4
E. coli ESBL 3	-	0.49	62.0	0.78×10^4	1.07×10^4
P. aeruginosa	-	0.97	15.54	1.07×10^4	1.07×10^4
E. coli	-	1.94	15.54	1.07×10^4	-
S. typhimurium	-	1.94	15.54	-	-
K. pneumonia	-	1.94	15.54	0.78×10^4	1.07×10^4
S. aureus	-	15.54	31.0	-	-

*Indicates no observed activities. Concentrations in μg mL^{-1}

First, we determined the conjugation percentage of lysozyme on the bioconjugates by Bradford protein assay and UV spectrophotometer at 595 nm. The quantity of lysozyme was determined using Equation 2 in the experimental section. The EE % of lysozyme in the bioconjugate is 98.35±0.170 % at pH 12. Then, we started the antibacterial experiments by evaluating the activities on the standard ATCC strains, and then we tested the resistant strains. The MIC estimation at the bacterial concentration of 5×10^5 CFU mL^{-1} showed a remarkable elevation in the antibacterial activity of AuNPs-lysozyme bioconjugate at very low concentrations compared to native lysozyme used at the same concentration of 1.43×10^4 μg mL^{-1} to construct the bioconjugate. MIC of the bioconjugate was 1.94 μg mL^{-1} against *E. coli* ATCC 25922, *K. pneumonia* ATCC 13833 and *S. typhimurium* ATCC 29629 and 15.54 μg mL^{-1} against *S. aureus* ATCC 29213 (Table 1). We tested the clinical resistant isolates on three ESBL-producing *E. coli* and one imipenem resistant *P. aeruginosa.* The MIC is 0.49 μg mL^{-1} against the three ESBL-producing *E. coli* and 0.97 μg mL^{-1} against imipenem resistant *P. aeruginosa* clinical isolates. Overall, MIC values were lower than those for the standard bacterial strains. This is in a sharp contrast with the native lysozyme and gold nanoparticles which did not inhibit all strains (Table 1).

AuNPs-lysozyme bioconjugate showed MBC of 62 μg mL^{-1} against the three ESBL-producing *E. coli* isolates, and 15.54 μg mL^{-1} against imipenem-resistant *P. aeruginosa*, *E. coli* ATCC 25922, *K. pneumonia* ATCC 13833 and *S. typhimurium* ATCC 29629; and 31.0 μg mL^{-1} against *S. aureus* ATCC 29213 (Table 1). Conclusive MIC and MBC studies indicate that gold nanoparticles bioconjugate is extremely bactericidal and effective against Gram-positive and Gram-negative bacteria at very low concentrations compared to native lysozyme. The antibacterial activity showed a better enhancement by 98-99% than the native lysozyme. Fleming and others suggested that lysozyme antibacterial activities are mainly against Gram-positive but not Gram-negative bacteria because they are protected by an outer membrane, which is relatively resistant to the catalytic hydrolysis by lysozyme.[4] The robust findings from our study supported the likelihood of lysozyme to extend its spectrum to Gram-negative superbugs. We showed that the antimicrobial activity against *P. aeruginosa* can be enhanced by the combination of the antibacterial activity of gold and lysozyme and is superior to that of native lysozyme. The conclusion from our study is supported by an investigation in

which peptidoglycan stabilized by gold nanoparticles was hydrolysed in the presence of lysozyme.[55]

3.4. Detection of bacterial DNA leakage

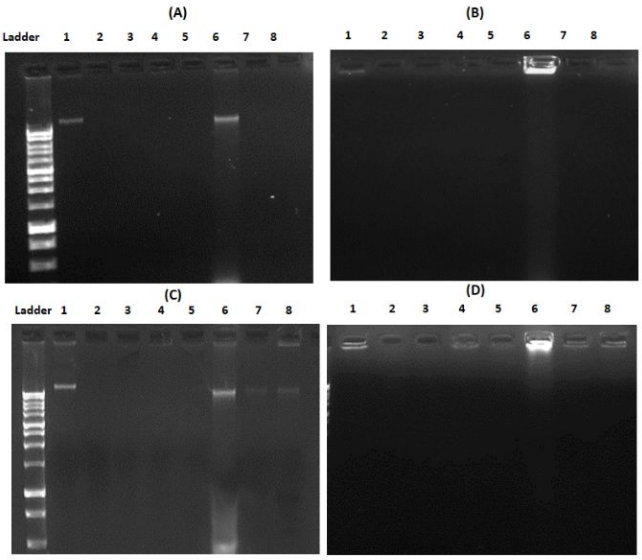

Fig. 5 Photographs of 1% agarose gel electrophoresis of bacterial samples genomic DNA after treatment with the bioconjugate and the native lysozyme for 1 and 3 h. Wells 1- 8 represent *S. aureus*, *E. coli*, *E. coli* ESBL 1, *E. coli* ESBL 2, *E. coli* ESBL 3, *P. aeruginosa*, *K. pneumoniae*, and *S. typhimurium* respectively. (A) After 1 h of incubation with AuNPs-lysozyme conjugate showed DNA bands in well 1 (*S. aureus*) and well 6 (*P. aeruginosa*). (B) After 1 h of incubation with native lysozyme, no DNA bands were observed. (C) After 3 h of incubation with AuNPs-lysozyme conjugate showed extra DNA bands in wells 7 (*K. pneumoniae*) and 8 (*S. typhimurium*). (D) After 3 h of incubation with native lysozyme, no DNA bands were observed.

Bacterial cell wall breakdown and DNA leakage by the action of lysozyme bioconjugate was detected by agarose gel electrophoresis. Samples incubated with the bioconjugate showed DNA bands for *Staphylococcus aureus* ATCC 29213 and *Pseudomonas aeruginosa* after 1 h of incubation. After 3 h of incubation, two more bands for *Salmonella typhimurium* ATCC 29629 and *Klebsiella pneumonia* ATCC 13833 were visible (Fig. 5). After 4 h of incubation, all strains including *E. coli* ATCC and ESBLs showed genomic DNA bands, however, no DNA bands were viewed from bacteria incubated with lysozyme (Fig. 5). This finding confirms cell wall break down by the action of the bioconjugate.

3.5. Nanoparticles adsorption to bacterial cell wall

Scanning electron microscopy is the most common technique used to probe the integrity and visualize the morphology of bacteria upon interaction with nanoparticles surface. ESBL *E. coli* strain 1 was treated with AuNPs-lysozyme bioconjugate and native lysozyme for 1 h to substantiate the adsorption of the positively charged nanoparticles-lysozyme to the surface of bacteria, and to view the physical morphological changes due to the exposure to both the bioconjugate and native lysozyme (Fig. 6). SEM images showed adsorption of the nanoparticles to the surface of bacteria. Carboxylic acid-terminated gold-aryl nanoparticles adsorbed to *E. coli* bacteria and resulted in morphological changes from rods to spheroplasts, in addition, fragmentation was observed. *E. coli* exposed to native lysozyme showed spheroplasts formation but no fragmentation (Fig. 6A). Spheroplasts formation designates physical damage of peptidoglycan by the action of lysozyme.[18,20,21] The integrity of the *E. coli* membrane as a permeability barrier was subsequently diminished (Fig. 6B). Functionalized gold-carbon nanoparticles, thus, are outstanding biointerface probes of the interaction between bacteria and surrounding surfaces.

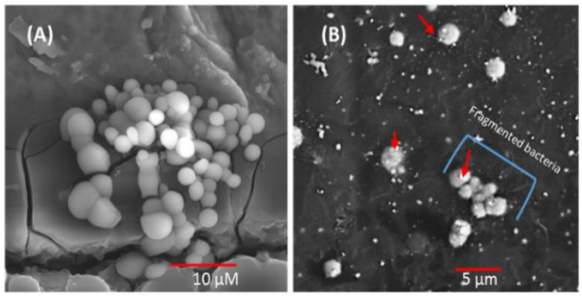

Fig. 6 SEM images of *E. coli* ESBL 1 showing integrity and morphological change upon the interaction with native lysozyme and gold-lysozyme bioconjugate. (A) Treated with lysozyme for 1 h showing spheroplasts formation, no fragmentation was observed. (B) Treated with AuNPs-lysozyme for 1 h showing fragmented spherical *E. coli* cells and nanoparticles adsorbed to the *E. coli* surface indicated by the arrows.

3.6. Viability of fibroblast and HeLa cancer cell lines and cellular morphological study

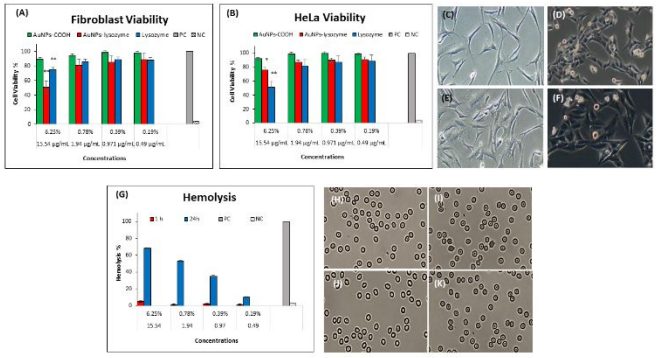

Fig. 7 (A,B) Cell viability of fibroblast and HeLa after 24 h of treatment with testing solutions at various AuNPs-lysozyme MICs. Concentrations are represented in percentage. The corresponding MICs of AuNPs-lysozyme are in µg mL^{-1}. Cross bars represent repeated standard errors ± of mean values of the replicates (n3). Samples statistically different from controls were marked (∗) for P-values < 0.05 and (∗∗) for P-values < 0.01. Phase contrast microscope images. (C,D) Fibroblast and HeLa control. (E,F) Fibroblast and HeLa treated with AuNPs-lysozyme at MIC of 1.94 µg mL^{-1} showing undamaged cells. (G) Hemolysis % after 1 and 24 h of incubation with AuNPs-lysozyme. Images of RBCs after 1 h of incubation with AuNPs-lysozyme. (H) Control in PBS. (I) MIC of 15.54 µg mL^{-1}. (J) MIC of1.94 µg mL^{-1}. (K) MIC of 0.97 µg mL^{-1}. The different concentrations showed normal, few haemolyzed and crenated RBCs.

In vitro studies were conducted to investigate the cytocompatibility of gold nanoparticles and their lysozyme bioconjugate on human fibroblast and HeLa cancer cells (Fig. 7A-B). We used skin fibroblast as a model for human cells and

probed the cytotoxicity of gold-lysozyme bioconjugate at selected MICs. Cytocompatibility results obtained using MTT assay after 24 h of contact with human cells. Primary Dermal Fibroblast Normal PCS-201-010 and HeLa CCL-2 cell lines demonstrated more than 50% and 76% viability when tested at the MIC value of Gram-positive *S. aureus* ATCC, respectively. While more than 80% of the cells were viable at the MICs values of Gram-negative ATCC strains and the used superbugs for both cell lines. AuNPs-COOH displayed no cytotoxicity at the selected MICs. Cells traded with native lysozyme displayed viability of 50 % and more at the used MIC for both cell lines. Cell viability results are displayed in Fig. 7, and the concentrations are represented as percentage of testing solutions and their corresponding MICs of the bioconjugate. According to our studies and literature works, gold nanoparticles synergistically act as antibacterial when loaded with lysozyme without a significant harm to the surrounding tissues. These findings indicate the selective toxicity of the bioconjugate. To estimate the effect of the bioconjugate on the cellular morphology of both fibroblast and HeLa cell lines, we assessed the changes after 24 h of treatment at a selected bioconjugate MIC of 1.94 μg mL^{-1} in DMEM medium using phase contrast microscope. No morphological changes were observed in both cell lines (Fig. 7C-F). In general, this study demonstrated that gold nanoparticles and their lysozyme bioconjugate can be tolerated by HeLa and fibroblast cells without morphological change or noteworthy cytotoxicity at the MICs. The low cell toxicity might be due to a few factors including the very low MICs, the amenable carboxyl terminated shell and the pure nanoparticles fabricated using a green approach.

3.8. Hemocompatibility study

Bacteraemia or blood stream related infections are detrimental. They often result in organ failure and high mortality rates. Antibacterial resistance is common against most Gram-negative bacterial strains in blood infection diseases.[7,9] Since gold-lysozyme bioconjugate is potent against superbugs, we studied its hemocompatibility under amenable MICs. Hemolysis assay was used to investigate the interaction between the gold-lysozyme bioconjugate and RBCs. Hemocompatibility was measured at MICs of 15.54, 1.94, 0.97 and 0.49 μg mL^{-1}. The quantitative change in the UV-Vis absorbance was followed at 575 nm after 1 and 24 h of incubation. The UV-Vis spectra of the bioconjugate after 1 h of incubation display negligible quantitative hemolysis of 1-5%, in addition, 1-2 % of haemolysed cells and few crenated RBCs were observed under microscope. However, the quantitative hemolysis increased considerably to 68%, 53%, 35% and 10% respectively after 24 h of incubation (Fig. 7G-K). These results indicate that hemolysis depends on the bioconjugate concentration. The observed hemocompatibility at the MICs for ESBLs *E. coli* and *P. aeruginosa* after long exposure is due to the very low concentrations, this makes the bioconjugate a potent drug to target internal organ infections and bacteraemia. Despite the quantitative increase of the hemolysis rate at high MICs, the bioconjugate can be applied on the superficial dermal infections due to minor cytotoxicity. The low hemolysis of the gold-lysozyme bioconjugate could be explained based on the passivation of the gold nanoparticles by the immobilized lysozyme. Bakshi demonstrated that masking the surface of nanoparticles by coating with biocompatible layer can significantly reduce their affinity to interact with blood cells.[56]

4. Conclusions

Lysozyme possesses antibacterial activity against some Gram-positive bacteria but little against Gram-negative bacteria due to the steric hindrance of the outer lipopolysaccharide layer which blocks the access to peptidoglycan. Fulfilling the synergistic principles into the design of the next generation therapeutics is a main target in the lysozyme-nanomaterials interface to reach antibiotic-free therapy. Gold nanoparticles and their enzyme bioconjugates have advantages over broad-spectrum antibiotics because superbugs will involve several gene mutations over a long period of time to develop resistance against gold-based nanoantibacterials. We were able to enhance the antibacterial activity of lysozyme by the conjugation with the robust gold-carbon nanoparticles. Moreover, the bioconjugate showed selective toxicity against bacteria over the mammalian cells. Our results are in support of the gold-lysozyme bioconjugate as a promising alternative treatment for ESBL and imipenem resistant bacteria. The bactericidal effect was induced even against the exceptionally low outer-membrane permeability of *P. aeruginosa* bacteria, which are known for their resistance to antibiotics. In addition, these findings showed lower MICs for the bioconjugate compared to the native enzyme.

Molecular docking results revealed that benzoic acid is bound into the deep buried enzyme active site and interacts with lysozyme through various kinds of interactions such as hydrogen bonding and hydrophobic including π-π T-shaped stacking. Thus, in accordance with the experimental results, our theoretical study has shown the binding of benzoic acid in the hydrophobic cavity of the protein thus exposing the positively charged hydrophilic surface to form strong electrostatic interaction with the negatively charged bacterial cell wall. The encouraging results of this work will catalyse the replacement of antibiotics with theranostics based on gold nanoparticles. Technological approaches can utilize our nanoplatform in which gel, cream or powder can be applied on infected wounds because of the absence of detrimental cytotoxicity to human cells.

Conflicts of interest

There are no conflicts to declare.

Acknowledgements

AAM acknowledges the University of Sharjah support of SEED grant (VC-GRC-SR-83-2015), competitive grants (160-2142-

029-P and 150-2142-017-P), Organometallic Research Group grant (RISE-046-2016) and Functionalized Nanomaterials Synthesis Lab grant (151-0039). AAM and BW acknowledge the support of Delaware State University Institute for Science and Technology. BW acknowledges the support of National Nuclear Security Administration (NNSA) grant number DE-NA0002683, Delaware State EPSCoR, CIBER, and Delaware State University Provisional Development Fund, Delaware Space Grant College Program and NASA Grant NNX15AI19H. CH acknowledges the support by INHA UNIVERSITY Research Grant (INHA-60121-1).

References

1 N. Cioffi and M. Rai (Eds), Nano-Antimicrobials: Progress and Prospects, *Springer-Verlag Berlin Heidelberg*, 2012, DOI: 10.1007/978-3-642-24428-5.
2 K. Kon and M. Rai, Antibiotic Resistance: Mechanisms and New Antimicrobial Approaches, *Elsevier Inc*, 2016.
3 R. Boukherroub, S. Szunerits and D. Drider, Functionalized Nanomaterials for the Management of Microbial Infection, *Elsevier Inc*., 2017.
4 A. Ficai and A. M. Grumezescu (Eds), Nanostructures for Antimicrobial Therapy, *Elsevier Inc*., 2017, DOI: 10.1039/9781849730990-00001.
5 Y. Zheng, W. Liu, Z. Qin, Y. Chen, H. Jiang and X. Wang, *Bioconjug. Chem*., 2018, **29**, 3094-3103, DOI: 10.1021/acs.bioconjchem.8b00452.
6 Y. Zhao, Z. Chen, Y. Chen, J. Xu, J. Li and X. Jiang. *J. Am. Chem*. Soc., 2013, **135**, 12940-12943, DOI: 10.1021/ja4058635.
7 K. P. Miller, L. Wang, B. C. Benicewicz and A. W. Decho, *Chem. Soc. Rev.*, 2015, **44**, 7787-7807, DOI 10.1039/C5CS00041F.
8 A. Amini, M. Kamali, B. Amini and A. Najafi, *J. Phys. D: Appl. Phys*., 2018, **52**, 065401. DOI: 10.1088/1361-6463/aaef4d/meta.
9 P. V. Baptista, M. P. McCusker, A. Carvalho, D. A. Ferreira, N. M. Mohan, M. Martins and A. R. Fernandes, *Front. Microbiol*., 2018, **9**, 1441, DOI: 10.3389/fmicb.2018.01441.
10 W. Y. Chen, H. Y. Chang, J. K. Lu, Y. C. Huang, S. G. Harroun, Y. T. Tseng, Y. J. Li, C. C. Huang and H. T. Chang, *Adv. Funct. Mater*., 2015, **25**, 7189-7199, DOI: 10.1002/adfm.201503248.
11 L. Aminlari, M. M. Hashemi and M. Aminlari, *J. Food Sci.*, 2014, **79**, R1077-R1090, DOI: 10.1111/1750-3841.12460.
12 B. Zhou, Y. Li, H. Deng, Y. Hu and B. Li, *Colloids Surf. B Biointerfaces*, 2014, **16**, 432-438. DOI: 10.1016/j.colsurfb.2014.01.016.
13 Y. Lee and K. E. Geckeler, *J. Biomed. Mater. Res*., 2012, Part A **100**, 848-855. DOI: 10.1002/jbm.a.34020.
14 M. Kiristi, V. V. Singh, B. E. de Ávila, M. Uygun, F. Soto, D. A. Uygun and J. Wang, *ACS Nano*, 2015, **9**, 9252-9259, DOI: 10.1021/acsnano.5b04142.
15 M. S. Bakshi, H. Kaur, T. S. Banipal, N. Singh and G. Kaur, *Langmuir*, 2010, **26**, 13535-13544, DOI: 10.1021/la101701f.
16 Y. M. Wang, C. C. Liu, Y. T. Zhang, B. Zhang and J. D. Liu, *Chem. Eng*., 2015, **3**, 1183-118, DOI: 10.1021/acssuschemeng.5b00104.
17 K. Meyer, J. W. Palmer, R. Thompson and D. Khorazo, *J. Biol. Chem*., 1936, **113**, 479-486. http://www.jbc.org/content/113/2/479.full.pdf
18 K. C. Huang, R. Mukhopadhyay, B. Wen, Z. Gitai and N. S. Wingreen, *PNAS*, 2008, **105**, 19282-7, DOI:10.1073/pnas.0805309105.
19 P. K. Chodisetti and M. Reddy, *PANS*, 2019, **116**, 7825-7830; DOI:10.1073/pnas.1816893116.
20 B. J. Bachmann and D. M. Bonner, *J. Bacteriol*., 1959, **78**, 550-556, https://jb.asm.org/content/78/4/550.long.
21 D. C. Birdsell and E. H. Cota-Robles*, J. Bacteriol*., 1967, **93**, 427-37, PMID: 4960155.
22 J. Su, W. Zhou, Y. Xiang, R. Yuan and Y. Chai, *Chem. Commun*., 2013, **49**, 7659-7661, DOI: 10.1039/C3CC43970D.
23 A. E. Enciso, G. Doni, R. Nifosi, F. Palazzesi, R. Gonzalez, A. A. Ellsworth, J. L. Coffer, A. V. Walker, G. M. Pavan, A. A. Mohamed and E. E. Simanek, *Nanoscale*, 2017, **9**, 3128-3132, DOI: 10.1039/c7nr90151h.
24 M. K. Hameed, I. M. Ahmady, H. Alawadhi, B. Workie, E. S. Demessie, C. Han, M. M. Chehimi and A. A. Mohamed, *Colloids Surf. A*, 2018, **558**, 351-358, DOI: 10.1016/j.colsurfa.2018.09.004.
25 A. A. Mohamed, S. N. Neal, B. Atallah, N. D. AlBab, H. A. Alawadhi, Y. Pajouhafsar, H. E. Abdou, B. Workie, E. S. Demessie, C. Han, M. Monge, J. M. Lopez-de-Luzuriaga, J. H. Reibenspies and M. M. Chehimi, *J. Organomet. Chem*., 2018, **877**, 1-11, DOI: 10.1016/j.jorganchem.2018.07.032.
26 S. Panicker, I. M. Ahmady, A. M. Almehdi, B. Workie, E. S. Demessie, C. Han, M. M Chehimi and A. A. Mohamed, *Appl. Organomet. Chem*., 2019, e4803, DOI: 10.1002/aoc.4803.
27 J. A. Pradeepkiran and P. H. Reddy, *Cells*, 2019, **8**, e260, DOI: 10.3390/cells8030260.
28 S. Vilar, E. Sobarzo-Sánchez and E. Uriarte, *Curr. Med. Chem*., 2019, **174**, 116-129. DOI: 10.2174/0929867325666171129121924.
29 S. K. Kashaw, S. Agarwal, M. Mishra, S. Sau and A. K. Iyer, *Curr. Comput.-Aid. Drug*, 2019, **15**, 55-66, DOI: 10.2174/1573409914666181015150731.
30 D. S. Goodsell, G. M. Morris and A. J. Olson, *J. Mol. Recognit.*, 1996, **9**, 1-5, DOI: 10.1002/(SICI)1099-1352(199601)9:1%3C1::AID-JMR241%3E3.0.CO;2-6.
31 J. Wang, M. Dauter, R. Alkire, A. Joachimiak and Z. Dauter, *Acta Crystallogr. D Biol. Crystallogr*., 2007, **63**, 1254-1268, DOI: 10.1107/S0907444907054224.
32 S. Kim, J. Chen, T. Cheng, A. Gindulyte, J. He, S. He, Q. Li, B. A. Shoemaker, P. A. Thiessen, B. Yu, L. Zaslavsky, J. Zhang and E. E. Bolton, *Nucleic Acids Res*., 2018, **47**, D1102-D1109, DOI: 10.1093/nar/gky1033.
33 C. Hetényi and D. van der Spoel, *Protein Sci*., 2002, **11**, 1729-1737, DOI: 10.1110/ps.0202302.
34 E. Jurrus, D. Engel, K. Star, K. Monson, J. Brandi, L. E. Felberg, D. H. Brookes, L. Wilson, J. Chen, K. Liles, M. Chun, P. Li, D. W. Gohara, T. Dolinsky, R. Konecny, D.R. Koes, J. E. Nielsen, T. Head-Gordon, W. Geng, R. Krasny, Guo-Wei Wei, M. J. Holst, J. A. McCammon and N. A. Baker, *Protein Sci.* 2018, **27**, 112-128, DOI: 10.1002/pro.3280.
35 D. Shugar, *Biochim. Biophys. Acta*, 1952, **8**, 302-309. PMID: 1493474.
36 R. Helal and M. F. Melzig, *Pharmazie*, 2008, **63**, 415-419, DOI: 10.1691/ph.2008.7846.
37 Clinical and Laboratory Standards Institute. Methods for Dilution Antimicrobial Susceptibility Tests for Bacteria That Grow Aerobically; Approved Standard Seventh Edition. CLSI document M7-A7 (ISBN 1-56238-587-9). Clinical and Laboratory Standards Institute, 940 West Valley Road, Suite 1400, Wayne, Pennsylvania 19087-1898 USA, 2006.
38 NCCLS document M26-A [ISBN 1-56238-384-1]. NCCLS, 940 West Valley Road, Suite 1400, Wayne, Pennsylvania 19087 USA, 1999.
39 N. González-Ballesteros, S. Prado-López, J. B. Rodríguez-González, M. Lastra and M. C. Rodríguez-Argüelles, *Colloids Surf. B Biointerfaces*, 2017, **153**, 190-198, DOI: 10.1016/j.colsurfb.2017.02.020.

40 M. R. Bindhu and M. Umadevi, *Mater. Lett*., 2014, **120**, 122-125, DOI: 10.1016/j.matlet.2014.01.108.
41 U. Kumara, A. K. Ranjan, C. Sharan, A. A. Hardikar, A. Pundle and P. Poddar, *Curr. Nanosci*., 2012, **8**, 130-140, DOI: 10.2174/1573413711208010130.
42 P. S. Belton and A. M. Gil, *Biopolymers*, 1994, **34**, 957-961, DOI: 10.1002/bip.360340713.
43 V. Polshettiwar and R. S. Varma (Eds.) Aqueous Microwave Assisted Chemistry: Synthesis and Catalysis, *RSC Publishing*, 2010, DOI: 10.1039/9781849730990-00001.
44 H. Cai and P. Yao, *Nanoscale*, 2013, **5**, 2892-2900, DOI: 10.1039/C3NR00178D.
45 A. F. Bravo, P. Sivakumar, N. Melikechi and A. A. Mohamed, *J. Nanosci. Nanotech*., 2017, **17**, 2852-2856, DOI: 10.1166/jnn.2017.13900.
46 W. Hui, F. Shi, K. Yan, M. Peng, X. Cheng, Y. Luo, X. Chen, V. A. Roy, Y. Cui and Z. Wang, *Nanoscale*, 2012, **4**, 747-751, DOI: 10.1039/C2NR11489E.
47 A. C. Pushkaran, N. Nataraj, N. Nair, F. Götz, R. Biswas and C. G. Mohan, *J. Chem. Inf. Model.*, 2015, **55**, 760-770, DOI: 10.1021/ci500734k.
48 T. Imoto, L. S. Forster, J. A. Rupley and F. Tanaka, *PNAS*, 1972, **69**, 1151-1155, DOI: 10.1073/pnas.69.5.1151.
49 Z. Gu, X. Zhu, S. Ni, Z. Su and H. M. Zhou, *Int. J. Biochem. Cell Biol*., 2004, **36**, 795-805, DOI: 10.1016/j.biocel.2003.08.015.
50 B. Saha, S. Chowdhury, D. Sanyal, K. Chattopadhyay and G. S. Kumar, *ACS Omega*, 2018, **3**, 2588-2601, DOI: 10.1021/acsomega.7b01991.
51 M. Zaman, H. A. Safdari, A. N. Khan, S. M. Zakariya, S. Nusrat, T. I. Chandel and R. H. Khan, *Int. J. Biolog. Macromol*., 2019, **134**, 1022-1037, DOI: 10.1080/07391102.2018.1547661.
52 R. Satishkumar and A. Vertegel, *Biotechnol. Bioeng.*, 2008, **100**, 403-412, DOI: 10.1002/bit.21782.
53 H. R. Luckarift, M. B. Dickerson, K. H. Sandhage and J. C. Spain, *Small*, 2006, **2**, 640-643, DOI: 10.1002/smll.200500376.
54 C. Garcia-Hernandez, A. K. Freese, M. L. Rodriguez-Mendez and A. K. Wanekaya, *Biomater. Sci*., 2019, **7**, 2511-2519, DOI: 10.1039/c9bm00129h.
55 F. Fu, L. Li, Q. Luo, Q. Li, T. Guo, M. Yu, Y. Song and E. Song, *Analyst*, 2018, **143**, 1133-1140, DOI: 10.1039/c7an01570d.
56 M. S. Bakshi. *Chem. Res. Toxicol*. 2017, **30**, 1253−1274. doi.org/10.1021/acs.chemrestox.7b00068.

TOC

The antibacterial functionalities of gold-carbon nanoparticles bioconjugate with lysozyme showed little or no damage against healthy human cells.